Semi-infinite boundary conditions for the simulation of interfaces: The Ar/CO_2(s) model revisited

Rocio de Gregorio,[1] Jorge Benet,[1] Nebil A. Katcho,[1,a)] Felipe J. Blas,[2] and Luis G. MacDowell[1,b)]
[1]*Departamento de Química Física, Facultad de Ciencias Químicas, Universidad Complutense, Madrid 28040, Spain*
[2]*Departamento de Física Aplicada, Facultad de Ciencias Experimentales, Universidad de Huelva 21071, Spain*

(Received 27 December 2011; accepted 19 February 2012; published online 13 March 2012)

We propose a method to account for the long tail corrections of dispersive forces in inhomogeneous systems. This method deals separately with the two interfaces that are usually present in a simulation setup, effectively establishing semi-infinite boundary conditions that are appropriate for the study of the interface between two infinite bulk phases. Using the wandering interface method, we calculate surface free energies of vapor–liquid, wall–liquid, and wall–vapor interfaces for a model of Lennard–Jones argon adsorbed on solid carbon dioxide. The results are employed as input to Young's equation, and the wetting temperature located. This estimate is compared with predictions from the method of effective interface potentials and good agreement is found. Our results show that truncating Ar–Ar interactions at two and a half molecular diameters results in a dramatic decrease of the wetting temperature of about 40%. © *2012 American Institute of Physics*. [http://dx.doi.org/10.1063/1.3692608]

I. INTRODUCTION

Whereas computer simulations are nowadays routinely employed as a means for materials modeling, there are still a number of long-standing issues that limit their scope. One such problem is the correct handling of van der Waals interactions at long distances. Typically, simulations account for explicit molecule–molecule interactions within a cutoff sphere of radius, R_c a few molecular diameters long. All other interactions beyond R_c are either completely ignored, or evaluated approximately within some *long tail-correction* scheme.[1,2] In bulk simulations of simple fluids, such corrections are easily and accurately evaluated by simply assuming the local density about a site is equal to the system's bulk density (hence, ignoring site–site correlations beyond R_c). In other cases, the situation is far more complicated, because, either the correlations are fairly long ranged (as in a semi-dilute polymer solution), or the local density is inherently non-homogeneous (as in the case of flat interfaces).

One case of great relevance where tail corrections need to be addressed with caution is the study of adsorbed fluids. It is well known that many relevant properties of adsorption and wetting behavior depend significantly on the range of interactions of the fluid–substrate pair.[3–6] In systems with van derWaals forces, for example, it is well known that adhesive fluid–wall interactions decay as the inverse cube.[7] Such power-law decay effectively accounts for van der Waals interactions between the fluid and the wall at all distances, without the need to explicitly sum an infinite number of pairwise interactions. Alas, such a simple prescription for cohesive fluid–fluid interactions does not exist. As a result, most studies of adsorbed fluids resort to a plain truncation of fluid–fluid forces, without any attempt to correct for the missing interactions.[8–18]

Already a while ago, Mansfield and Theodorou pointed out that truncating r^{-6} fluid–fluid interactions in systems where a z^{-3} fluid–wall potential is employed would have the effect of considerably favoring adhesive over cohesive interactions, and hence, very much affect the work of adhesion of adsorbed polymer films.[19,20] In order to remedy this problem, they developed a method for the calculation of tail corrections of adsorbed fluids. This method implies a slice by slice summation of dispersive interactions stemming from thin sheets of infinitesimal width parallel to the substrate, with such interactions weighted by the local density of each sheet.

This procedure has been employed since then in a few instances,[21–28] either for the study of adsorbed fluids,[23,24] or free interfaces,[21,22,25–28] both in molecular dynamics[21,22,24] and Monte Carlo simulations.[25–28] However, we note here that the correct calculation of long tail forces for use in molecular dynamics simulations needs extra caution, as described recently.[25,28] It is also worth mentioning that alternative procedures for the evaluation of tail corrections in inhomogeneous systems are known,[29–32] but the one suggested by Mansfield and Theodorou is possibly the most natural and less time consuming.

Proper calculation of tail corrections as discussed above has shown a very important contribution to surface free energies, both for adsorbed fluids and liquid–vapor interfaces. Considering that very important properties of adsorbed films, such as the wetting temperature, are determined by a balance of such free energies, it is natural to ask to what point could the wetting temperature be affected by the neglect of tail corrections.

a)Also at LITEN, CEA-Grenoble, 17 rue des Martyrs, 38054 Grenoble Cedex 9, France.
b)Author to whom correspondence should be addressed. Electronic mail: luis@ender.quim.ucm.es.

Among all choices of fluid–substrate pairs, the model of argon adsorbed on solid CO_2 first suggested by Ebner and Saam in their work on the prewetting transition is perhaps the most widely studied, both in terms of theoretical[11,33–37] and simulation approaches.[9–13,15,38–41] In the context of this work, such model is actually of great interest, since the wall–fluid potential is of the 9–3 type, and most computer simulations have applied plain truncation of the argon potential at $R_c = 2.5\sigma$, ever since Finn and Monson first found evidence for the prewetting transition.[9–13,15,38–41] Whereas the first computer simulation studies suggested a wetting temperature of about $k_B T_w/\epsilon = 0.85$, more recent studies have been decreasing this estimate gradually to the presently most reliable value of about $k_B T_w/\epsilon = 0.60$.[13] Intriguingly, the only simulation study that attempted to incorporate to some extent the tail corrections (using a minimum image convention) suggested a much higher wetting temperature of $k_B T_w/\epsilon = 0.95$.

The goal of this paper is twofold. First, we suggest a method to account for tail corrections which implicitly imposes in the simulated interfaces the semi-infinite boundary conditions that are appropriate for the calculation of surface tensions. This method is largely based on that suggested by Mansfield and Theodorou and others,[20,21,25] but adds extra corrections which improve the description and reduce the computational cost. Second, we apply the new boundary conditions in order to clarify the role of neglected tail corrections in the wetting temperature of the Ar/CO_2 model.

II. LONG TAIL CORRECTIONS

Consider a tetragonal simulation box, with an elongated side of length D along the z direction, and two equal shorter sides of length L along the x and y directions. For systems that are inhomogeneous and exhibit two interfaces, we will henceforth assume the inhomogeneity runs in the direction of the z axis.

The energy felt by species i due to interactions beyond the cutoff distance may be expressed in terms of the instantaneous density profile as

$$U_i^{ltc} = \int_{V \ni \mathfrak{S}(R_c, \mathbf{r}_i)} \rho(\mathbf{r}) u(\mathbf{r}_i, \mathbf{r})\, \mathrm{d}\mathbf{r}, \tag{1}$$

where $\mathfrak{S}(x, y)$ is a sphere of radius x centered at y. Starting from this equation, one may obtain different long tail corrections (LTC) depending on the assumption that is made for $\rho(\mathbf{r})$ within the domain of integration.

A. Spherical shell summation

In the case of a bulk phase, one may assume that correlations beyond R_c have vanished, so that $\rho(\mathbf{r})$ equals the bulk density outside $\mathfrak{S}(R_c, \mathbf{r}_i)$. The resulting integral can then be easily calculated in spherical coordinates, yielding the well-know result for the Lennard–Jones potential,

$$U_i^{ltc} = \frac{16\pi}{3} \rho_b \sigma^3 \epsilon \left\{ \frac{1}{3} \left(\frac{\sigma}{R_c} \right)^9 - \left(\frac{\sigma}{R_c} \right)^3 \right\}, \tag{2}$$

where σ and ϵ are the size and energy parameters of the LJ potential, while ρ_b is the bulk density. We will henceforth name this LTC, as SSS-LTC, for spherical shell summation.

B. Parallel slice summation

For the case of a liquid–vapor or fluid–substrate interface, an inhomogeneous density profile perpendicular to the interface results (say, along z). In a mean field sense we may assume ρ is a function of z only, so that the volume integration is best performed as a sum over parallel slabs,

$$U_i^{ltc} = \int_{-\infty}^{\infty} \rho(z) \left\{ \int_{\mathbf{r}_\parallel \ni \mathfrak{C}(r_\parallel^{min}, z_i)} u(\mathbf{r}_i, \mathbf{r})\, \mathrm{d}\mathbf{r}_\parallel \right\} \mathrm{d}z, \tag{3}$$

where $\mathfrak{C}(x, y)$ is a circle of radius x centered at y and $r_\parallel^{min} = (R_c^2 - (z - z_i)^2)^{1/2}$ for $R_c^2 > (z - z_i)^2$ and zero otherwise.

For the special case of the Lennard–Jones potential, the term in brackets may be integrated right away using cylindrical coordinates, leading to[25]

$$U_i^{ltc} = \int_{-\infty}^{\infty} \rho(z) w(z - z_i)\, \mathrm{d}z \tag{4}$$

with

$$w(z) = \begin{cases} 4\pi\sigma^2\epsilon \left[\frac{1}{5}(\sigma/R_c)^{10} - \frac{1}{2}(\sigma/R_c)^4 \right] & z \le R_c \\ 4\pi\sigma^2\epsilon \left[\frac{1}{5}(\sigma/z)^{10} - \frac{1}{2}(\sigma/z)^4 \right] & z > R_c \end{cases}. \tag{5}$$

The total energy arising from long tail corrections is then given as a sum over individual contributions, with a factor 1/2 not to include mutual interactions twice

$$U^{ltc} = \frac{1}{2} \sum_i \int_{-\infty}^{\infty} \rho(z) w(z - z_i)\, \mathrm{d}z. \tag{6}$$

The above expression may be evaluated by discretization of the z coordinate and evaluation of the density inside slices centered at nodes z_k. This strategy, which we will henceforth name as PSS-LTC, for parallel slice summation, has been employed by different authors for the calculation of bound[19,20,23,24] and free interfaces.[25–28]

The procedure, however, turns out to be somewhat awkward, particularly in the case of molecular systems, where each displacement will involve changes in the long tail corrections of all the molecular sites. Alternatively, the above equation may be rewritten as a sum of pairwise interactions. This can be achieved by recalling

$$\rho(z) = \frac{1}{A} \sum_j \delta(z - z_j), \tag{7}$$

where $A = L^2$ is the area of the surface perpendicular to the interface.

Substitution of this equation into Eq. (6), followed by integration along z yields:

$$U^{ltc} = \frac{1}{2A}\sum_i \sum_j w(z_j - z_i). \tag{8}$$

The unrestricted summation over i and j indices can be finally transformed into a sum of pair and *self* terms

$$U^{ltc} = \frac{1}{A}\sum_i \sum_{j>i} w(z_j - z_i) + \frac{1}{2A}\sum_i w(0). \tag{9}$$

This result corresponds to the exact evaluation of Eq. (6), with no need for discretization. Surprisingly, it corresponds to the addition of an extra effective pair potential evaluated within the minimum image convention along the z direction. Furthermore, the above expression has some desirable features. It is easily implemented within a computer code, it does not need on the fly evaluation of density profiles and it may actually become more efficient to evaluate than the discretized counterpart of Eq. (6) when large simulation boxes are employed. Note that as long as the surface area remains unchanged, the self term is a constant. Hence, attempted displacements will only involve the effective pair interactions. On the contrary, changes of the self-term must be accounted for when the simulation box is deformed.

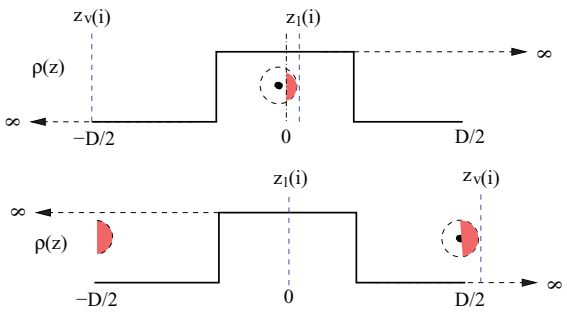

FIG. 1. Illustration of the semi-infinite boundary conditions. Full lines indicate the actual density profile in the simulation box, with molecules in the finite interval [-D/2,D/2] and a liquid slab about $z = 0$. Horizontal dashed lines indicate a continuous extrapolation of the bulk densities. Top figure shows semi-infinite boundary conditions for a molecule in the interval [-D/2,0] (*left interface*). A molecule less than R_c away from $z = 0$ feels explicit Lennard–Jones interactions within the cutoff sphere (including those of molecules with $z > 0$ contained in the shadowed red region), plus the effective slab potential with all molecules in the interval $[z_v(i), z_l(i)]$ and semi-infinite slabs of vapor and liquid density at $z_v(i)$ and $z_l(i)$, respectively. Bottom figure shows semi-infinite boundary conditions appropriate for molecules in the interval [0, D/2] (*right interface*). A molecule less than R_c away from $z = D/2$ feels explicit Lennard–Jones interactions within the cutoff sphere, thus interacting with molecules at $z = -D/2$ across the boundary conditions (as depicted in the shaded red region). The effective slab potential is felt with all molecules in the interval $[z_l(i), z_v(i)]$, while semi-infinite slabs of liquid and vapor density are felt at $z_l(i)$ and $z_v(i)$, respectively.

C. Semi-infinite boundary conditions

Ideally, surface tension calculations should be performed in a system with a single interface, containing two semi-infinite slabs of, say, vapor to the left and liquid to the right. Thus, Eq. (6) would be interpreted as having an asymptotic vapor profile towards $z = -\infty$ and an asymptotic liquid profile towards $z = \infty$.

Actually, one has a finite simulation box with periodic boundary conditions, the integration ranges from $-D/2$ to $D/2$ and two interfaces are present. Thus, using long tail corrections as in Eq. (6) a molecule in the middle of the liquid phase will feel the presence of two interfaces, instead of a single interface to the left and a semi-infinite liquid slab to the right (cf., Fig. 1–top).

Of course, this situation could be remedied by employing a sufficiently large system, such that the two interfaces are infinitely apart. A molecule located in the left interface of the simulation box would effectively feel a semi-infinite vapor slab as the result of interactions with distant molecules to the left of the interface, and a liquid semi-infinite slab with molecules sufficiently to the right.

In practice, this situation can be mimicked with a finite system by using periodic boundary conditions for interactions within a cutoff distance only, while employing semi-infinite boundary conditions for the long tail corrections.

This can be achieved by considering the molecules within the interval $[-D/2, 0]$ to belong to the "left" interface, and those in the interval $[0, D/2]$ to belong to the "right" interface (Fig. 1).

Molecules belonging to the left interface are assumed to feel an asymptotic vapor profile beyond $z = -D/2$, and an asymptotic liquid profile beyond $z = 0$ (Fig. 1–top). The long tail interaction felt by molecule i in the left interface is then

$$U_i^{ltc} = \rho_v \int_{-\infty}^{z_v(i)} w(z - z_i)\,\mathrm{d}z + \int_{z_v(i)}^{z_l(i)} \rho(z) w(z - z_i)\,\mathrm{d}z + \rho_l \int_{z_l(i)}^{\infty} w(z - z_i)\,\mathrm{d}z, \tag{10}$$

where the integral bounds $z_v(i)$ and $z_l(i)$ correspond to effective limits beyond which molecule i feels semi-infinite vapor and liquid slabs, respectively.

Within the finite simulation box, such bounds may be taken as

$$z_v(i) = \min(-D/2, z_i - R_c),$$
$$z_l(i) = \max(z_i + R_c, 0). \tag{11}$$

These limits are chosen so as to ensure that all molecules in the interval $[-D/2, 0]$ explicitly interact with neighbors inside their cutoff sphere. Therefore, a molecule less than R_c away from 0 explicitly interacts with those molecules beyond $z = 0$ that fall inside its cutoff distance (Fig. 1–top). All remaining interactions with molecules further apart are taken into account effectively by means of the slab potential under the assumption of constant liquid density. Similarly, a molecule less than R_c away from $-D/2$ will explicitly interact with molecules beyond $z = -D/2$ across the periodic boundary conditions. The remaining interactions with molecules well inside the fictitious semi-infinite vapor phase are taken into account with the slab potential under the assumption of constant vapor density.

Similarly, a molecule i pertaining to the right interface, will feel interactions of the form,

$$U_i^{ltc} = \rho_l \int_{-\infty}^{z_l(i)} w(z - z_i)\,\mathrm{d}z + \int_{z_l(i)}^{z_v(i)} \rho(z) w(z - z_i)\,\mathrm{d}z + \rho_v \int_{z_v(i)}^{\infty} w(z - z_i)\,\mathrm{d}z, \tag{12}$$

where now the effective limits $z_v(i)$ and $z_l(i)$ are given by

$$z_l(i) = \min(0, z_i - R_c),$$
$$z_v(i) = \max(z_i + R_c, D/2). \tag{13}$$

Again, these limits are chosen so as to ensure that all molecules in the interval $[0, D/2]$ explicitly interact with neighbors inside their cutoff sphere. Therefore, a molecule less than R_c away from $D/2$ will explicitly interact with molecules beyond $D/2$ across the periodic boundary conditions. The remaining interactions with molecules well inside the fictitious semi-infinite liquid phase are taken into account with the slab potential under the assumption of constant vapor density (Fig. 1–bottom).

The first and third integrals of Eq. (10) and Eq. (12) amount to a semi-infinite slab strength,

$$w_s^{\infty}(z) = \int_z^{\infty} w(z')\,\mathrm{d}z', \tag{14}$$

and may be readily evaluated for the LJ potential, yielding

$$w_s^{\infty}(z) = \frac{2\pi}{3}\sigma^3\epsilon \left\{ \frac{2}{15}\left(\frac{\sigma}{z}\right)^9 - \left(\frac{\sigma}{z}\right)^3 \right\}. \tag{15}$$

The second integral of Eq. (10) and Eq. (12) may be computed as in the PSS strategy described before, taking into account that the pairwise summation now runs over particles inside the effective limits $z_v(i)$ and $z_l(i)$. It is thus found that species pertaining to the left interface carry an energy of

$$U^{ltc}(z_i) = \frac{1}{A} \sum_{\substack{j \in [z_v(i),\, z_l(i)] \\ j \neq i}} w(z_j - z_i) + \rho_v w_s^{\infty}(z_i - z_v(i)) + \rho_l w_s^{\infty}(z_l(i) - z_i) + \frac{w(0)}{A} \tag{16}$$

with limits taken from Eq. (11). On the other hand, species belonging to the right interface have an energy of

$$U^{ltc}(z_i) = \frac{1}{A} \sum_{\substack{j \in [z_l(i),\, z_v(i)] \\ j \neq i}} w(z_j - z_i) + \rho_l w_s^{\infty}(z_i - z_l(i)) + \rho_v w_s^{\infty}(z_v(i) - z_i) + \frac{w(0)}{A} \tag{17}$$

with limits taken from Eq. (13).

If a molecule j belongs to the interval $[z_v(i), z_l(i)]$, it must also follow that molecule i belongs to the interval $[z_v(j), z_l(j)]$. Therefore, any interaction $w(z_j - z_i)$ is felt twice, and the full long tail energy with the proposed semi-infinite boundary conditions is given as

$$U^{ltc} = \frac{1}{A} \sum_i \sum_{\substack{j > i \\ j \in [z_v(i),\, z_l(i)]}} w(z_j - z_i) + \frac{1}{2} \sum_i \times \left\{ \rho_v w_s^{\infty}(z_v(i) - z_i) + \rho_l w_s^{\infty}(z_i - z_l(i)) + \frac{w(0)}{A} \right\}. \tag{18}$$

Compared to Eq. (9), we notice that the expensive double summation over the effective slab potential w is now considerably reduced because only interactions within roughly half a box need be considered. On the other hand, the self-term now becomes position dependent, clearly favoring molecules close to the semi-infinite liquid slab. Therefore, the semi-infinite boundary conditions may be regarded as a conceptually meaningful device as well as a protocol for reducing computational costs.

Unfortunately, in practice we find that these procedure is quite tricky to implement for the case of MC simulations of free interfaces (i.e., liquid–vapor interfaces). The reason is that a liquid slab placed initially at the center of the simulation box undergoes a random walk, so that eventually all of the liquid slab may be found at one side of the simulation box. Setting external fields mimicking the bulk liquid at the center of the box then do not longer make any sense. Essentially, the problem is that one cannot find the right location for a field in a system that is meant to be translationally invariant. Surprisingly, we found that the external fields are not strong enough to pin the liquid slab. The alternative of dynamically changing the origin of the simulation box is not convenient, since this will either dangerously affect the Markov chain if the energy change is not taken into account; or alternatively, would imply recalculating the energy globally (for all the system) at each local move.

The semi-infinite boundary condition (SBC) may still be exploited to great advantage for systems which are not translationally invariant, however, i.e., for fluids adsorbed at a wall, where typically the wall is actually simulated as a symmetric slit pore. Eqs. (16) and (18) may be then still employed, with the only caution of removing the semi-infinite potentials that fall within the space of the substrate.

III. MODEL AND SIMULATIONS

A. Wandering interface method

The wandering interface method (WIM) is a very robust technique which allows to calculate surface free energies for both free and bound interfaces.[42] In this method, a conventional Monte Carlo simulation is supplemented with an additional movement consisting in the change of the breadth to width ratio of the simulation box at constant volume. In this way, deformations of the lateral, L, and perpendicular, D, dimensions of the simulation box are coupled so as to probe effectively the anisotropy of the pressure tensor. Since an interface has a high energy cost, the system will spontaneously elongate in order to decrease the surface area. Due to thermal fluctuations, however, this transformation proceeds

in a random manner, and the resulting probability distribution of the interface area allows one to extract the surface free energy.

In practice, the WIM attempt is performed every many local moves or cycles. At the end of each cycle, a random area increment is chosen uniformly from a preset interval $[-\Delta_{max}, \Delta_{max}]$ and a new trial area $A_n = A_o + \Delta$ is proposed. The new box parameters are then transformed to $L_n = A_n^{1/2}$ and $D_n = V/A_n$. The attempted move is accepted with probability,

$$P_{acc} = \min(1, e^{-\beta(U_n - U_o + W_n - W_o)}), \tag{19}$$

where U is the system's energy and o/n sub-indices stand for variables before and after the attempt. W is a weighting function whose goal is to prevent the random surface area walk to move away from reasonable bounds. In practice, the most convenient choice for W is a bracketing function, i.e.,

$$e^{-\beta W(A)} = \begin{cases} 0 & A < A_{min} \\ 1 & A_{min} < A < A_{max} \\ 0 & A > A_{max} \end{cases}. \tag{20}$$

With this choice of weight function, WIM produces an unconstrained probability distribution of the interface area within the preset bounds $[A_{min}, A_{max}]$, i.e.,

$$f(A) = e^{-\beta(2\gamma A - p_\perp V)}, \tag{21}$$

where γ is the surface tension and $p_\perp$ is the component of the pressure tensor perpendicular to the interface.

1. Free interfaces

For liquid–vapor interfaces, WIM is implemented within a *NVT* MC simulation. The simulation box is prepared so as to accommodate a liquid slab surrounded by two vapor phases. In this situation, the system is found spontaneously in phase equilibrium, and $p_\perp$ is constant throughout the simulation and equal to the vapor pressure. The surface tension can be therefore extracted immediately from the slope of $\ln f(A)$.

Typically, our simulations where performed inside a cuboidal box with average surface area of $A = 180$ (hence, lateral size $L = 13.4\sigma$) and length $D = 44\sigma$, containing $N = 2137$ molecules. Box deformations are bracketed such that the surface area fluctuates within $\pm\Delta A_{max}$, with ΔA_{max} ranging from $1\sigma^2$ for the lowest temperature to $7\sigma^2$ for the highest temperature. The LJ potential is truncated at $R_c = 2.5\sigma$ and tail corrections are evaluated using the PSS technique (when relevant). Simulations are performed for 1×10^6 cycles. A cycle consists of N canonical MC moves, followed by a WIM attempt. Canonical MC moves consisted of usual Metropolis translations, and configurational bias displacements of the center of mass in a ratio 1:1. The outcome of the simulations is the probability distribution of surface areas, as well as the liquid–vapor density profile. Bulk coexistence densities are extracted from these profiles for use in the subsequent simulations for bound interfaces under SBC. A bulk *NVT* simulation of the vapor phase is also performed, and the coexistence chemical potential determined by means of the test particle method.[2]

2. Bound interfaces

For bound interfaces, a fluid phase (either vapor or liquid) is confined within a simulation box with walls located at $z = \pm D/2$. In this case, MC sampling must be performed within a grand canonical ensemble, since box deformations would otherwise change the system's bulk density. Also note one actually simulates a slit pore, so that both γ and $p_\perp$ pick up in principle a non-trivial slit pore width dependence.[42–44] Fortunately, these dependency rapidly decays to asymptotic values for pore widths larger than the interfacial width. Therefore, it is required to perform preliminary simulations for a few pore widths in order to check $p_\perp$ has reached its asymptotic value (i.e., the bulk fluid pressure at that chemical potential). Once this condition is met, the simulations may be safely performed and again the surface tension is extracted from the slope of $\ln f(A)$.

For bound interfaces, simulations were performed in the grand canonical ensemble with chemical potentials determined from test particle insertions of the bulk vapor phase (see above). Semi-infinite boundary conditions were employed, with input densities determined from the liquid–vapor simulations. Different simulation boxes were considered depending on the fluid phase. Liquid–wall interfaces were simulated in a box with a lateral area of about $130.5\sigma^2$, and $D = 31\sigma$, while WIM sampling was allowed within an interval of $1\sigma^2$ to $2\sigma^2$ depending on the temperature. For wall–vapor interfaces, the simulation box had a lateral area of $158\sigma^2$ and a large $D = 140\sigma$ required to avoid capillary condensation. Alternatively, smaller perpendicular distances may be employed by rejecting grand canonical attempts that fill the simulation box beyond some prescribed value. WIM sampling was performed for these systems within intervals of size 2 to 4 σ^2.

Simulations are performed over 1×10^6 cycles, with cycles defined as 3000 molecular displacements followed by one WIM attempt. Molecular displacements include center of mass translation and grand canonical configurational bias insertion (cf. Ref. 45) in the ratio 1:1.

B. Effective interface potentials

In mean field theory, an interface potential is the surface free energy of an adsorbed film as a function of film thickness. Following previous work on homogeneous bulk and inhomogeneous systems,[46,47] we have recently extended the calculation of coarse grained free energies by molecular simulations in order to obtain *effective* interface potentials for the study of interfacial phenomena.[14,48] In this method, one simulates an adsorbed film in the grand canonical ensemble and collects the probability of finding N molecules inside that half box pertaining to the substrate, $P_{1/2}(N)$. The number of molecules is transformed into an adsorption, $\Gamma = (N - \frac{1}{2}\rho_v V)/A$, and an effective interface potential is simply calculated using

$$g(\Gamma) = -\frac{k_B T}{A} \ln P_{1/2}(N). \tag{22}$$

The method is not as trivial as suggested by this explanation, since one actually needs to sample all possible states

between a thin and a sufficiently thick film. For this reason, special sampling techniques are required. In this work we have employed transition matrix Monte Carlo.[49] This is a powerful technique which exploits information from rejected MC attempts in order to built the histogram $P_{1/2}(N)$. The extension of this method to the grand canonical ensemble has been largely documented and we refer the reader to that work for further details.[13,41]

The simulations where performed inside a box with dimensions $L = 10\sigma$ and $D = 50\sigma$, placing an adsorbing wall in one side and a purely repulsive wall in the other. The LJ potential is truncated at $R_c = 2.5\sigma$ and tail corrections are evaluated using SBC, with the semi-infinite fields acting only on one side of the simulation box. Typical simulations are performed in batches consisting of 10^8 ordinary grand canonical insertion/deletion attempts, with probability histograms recalculated every 10^6 moves. Between 300 and 10000 batches were sent for each temperature.

C. The model

In order to test the role of neglected tail corrections in the adsorption behavior, we consider the well-known model of Ar adsorbed on solid CO_2, first studied by Ebner and Saam.[33] In this model, Ar is described using a Lennard–Jones potential with ϵ and σ range and energy parameters, respectively, while the solid CO_2 substrate is effectively accounted for by an external potential which only depends on the perpendicular distance of the adsorbed Argon atoms to the solid's first layer, z:

$$V_s^{\infty}(z) = \frac{2\pi}{3}\sigma_{wf}^3\rho_w\epsilon_{wf}\left\{\frac{2}{15}\left(\frac{\sigma_{wf}}{z}\right)^9 - \left(\frac{\sigma_{wf}}{z}\right)^3\right\}, \quad (23)$$

where $\sigma_{wf} = 1.096\sigma$ and $\epsilon_{wf} = 1.277\epsilon$ are the wall–fluid parameters, while $\rho_w\sigma_{wf}^3 = 0.988$ is the substrate's reduced density. This potential is obtained by assuming a semi-infinite bulk phase of Lennard–Jones atoms placed between $-\infty$ and 0, followed by summation of the potential all such atoms generate at a point z away from the origin. No wonder, the resulting field is exactly as that of a semi-infinite slab (cf., Eq. (15)), with the only difference that the Lennard–Jones parameters now correspond to the pair interaction between Ar and CO_2 molecules.

IV. RESULTS

A. Test of the semi-infinite boundary conditions

As a first test of the SBC proposed in this work, we performed bulk *NVT* simulations for the LJ potential at a supercritical temperature ($k_BT/\epsilon = 2\epsilon$) and three different densities ($\rho\sigma^3 = 0.2$, 0.4, and 0.8). The simulations were carried out in a cubic box with side $L = D = 10\sigma$. In all cases, explicit interactions were evaluated for molecules within a cutoff sphere of radius $R_c = 2.5\sigma$, with the remaining energy contributions evaluated employing the usual SSS, as well as with PSS and SBC. Note that in the PSS and SSS methods, the LTC need to be considered in the acceptance criteria, so that a different series of simulations was launched for each method.

TABLE I. Internal energy per molecule as obtained for the LJ model at $k_BT/\epsilon = 2$ in a cubic simulation box of side $L = 10\sigma$ using different methods to evaluate LTC. Second to fourth columns are data for LJ monomers, while fifth to seventh are for LJ dimers. The entry under PSS′ corresponds to results of PSS with the system size correction of Eq. (25) added.

$\rho\sigma^3$	0.2	0.4	0.8	0.2	0.4	0.6
$-\beta$ U/N (SSS)	0.6499	1.2681	2.3805	2.3167	4.5842	4.0241
$-\beta$ U/N (PSS)	0.6484	1.2651	2.3729	2.3082	4.5728	3.9708
$-\beta$ U/N (SBC)	0.6504	1.2686	2.3807	2.3147	4.5857	4.0244
$-\beta$ U/N (PSS')	0.6501	1.2684	2.3796			

Table I gathers the results for the average internal energy per molecule obtained in the simulations. Comparing the first and third row of the table shows that SBC reproduces with great accuracy the results that are obtained from the usual bulk SSS. Indeed, both schemes sum all possible interactions beyond the cutoff sphere up to infinity, only differing in the way the summation is performed.

On the contrary, a small but significant difference between PSS and SSS corrections is apparent in all cases, with PSS corrections providing a somewhat smaller internal energy than either SSS or SBC corrections. The reason for these discrepancy is that long tail corrections evaluated by means of PSS employ periodic boundary conditions for the slice summation. Accordingly, the LTC are not summed up to infinity. Rather, only contributions from molecules at a distance $z \le D/2$ are actually included.

The energy felt by molecule i amounts to

$$U_i = \frac{1}{2}\int_{-D/2}^{D/2}\rho(z)w(z)\,\mathrm{d}z. \quad (24)$$

Substitution of Eq. (5) into the above integral, shows, after some manipulations, that the energy per molecule actually felt using PSS is

$$\frac{U^{ltc}}{N} = \frac{8\pi}{3}\rho_b\sigma^3\epsilon\left\{\frac{1}{3}\left(\frac{\sigma}{R_c}\right)^9 - \left(\frac{\sigma}{R_c}\right)^3\right\} + \frac{4\pi}{3}\rho_b\sigma^3\epsilon \times \left\{\frac{1}{15}\left(\frac{\sigma}{D/2}\right)^9 - \frac{1}{2}\left(\frac{\sigma}{D/2}\right)^3\right\}. \quad (25)$$

Taking the limit of $L \to \infty$, we recover the well known result of SSS–LTC. For finite boxes, however, a small difference of order D^{-3} results.

In order to make this point apparent, Table I includes an extra row where the D dependent correction calculated above, is added to the simulated energies obtained with the PSS method. Clearly, adding the missing term in the PSS scheme brings all three methods in very close agreement.

As another test of the SBC proposed in this work, we plot density profiles of the LJ fluid, $\rho(z)$ obtained in the course of the *NVT* simulations (Fig. 2). The figure clearly displays smooth and flat density profiles within the simulation box all the way from $-D/2 < z < D/2$. This shows that the position dependent external fields correctly mimic the role of bulk semi-infinite slabs, and do not produce any spurious effect. In particular, no sign of discontinuity or oscillations, either at the box limits or in the box center, $z = 0$ are observed.

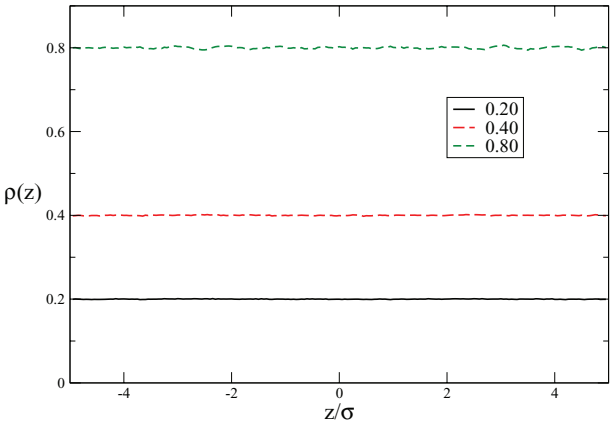

FIG. 2. Density profiles of a bulk Lennard–Jones fluid using SBC. No discontinuities or oscillations are observed either at the center of the simulation box, $z = 0$ or at the sides $z = \pm D/2$.

Obviously, the success of the procedure relies on correctly introducing the target densities to use with the semi-infinite slab potentials (cf., Eqs. (16) and (18)). This requirement seems a very low price to pay for avoiding the problem of periodic boundary conditions. Recently, Attard suggested a procedure for avoiding periodic boundary conditions which is based on imposing hard walls at the box sides, and adding an effective many body potential that is meant to suppress the fluid–wall correlations.[50] The method works well for low densities, but is unable to avoid density oscillations close to the wall for typical liquid densities. On the contrary, the SBC avoid altogether density oscillations at a much lower computational cost, even at considerably high bulk densities. SBC achieves this because the slab potential, which is also very steep at $z = 0$ and would therefore create spurious oscillations, is always evaluated at distances larger than a safety distance R_c.

Having tested the performance of SBC for the case of bulk fluids, let us now consider inhomogeneous fluids, where

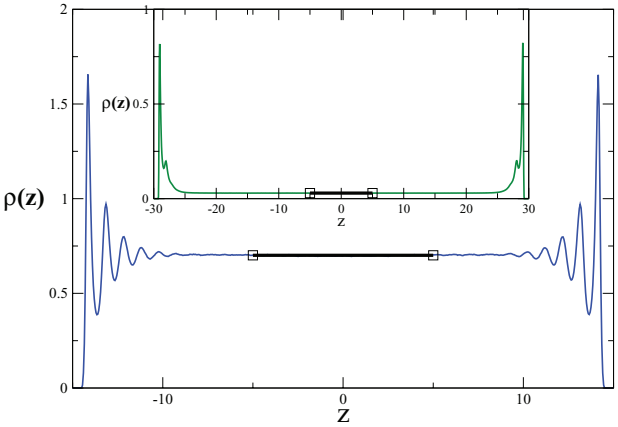

FIG. 3. Density profiles for the wall–liquid interface of Ar adsorbed on CO_2 at temperature $k_BT/\epsilon = 1.00$ and coexistence conditions, with tail corrections evaluated using SBC. The inset shows results for the wall–vapor interface. No discontinuities or oscillations are observed at the center of the simulation box, $z = 0$. Thick black horizontal lines indicate the asymptotic densities expected from bulk coexistence as reported in Ref. 51.

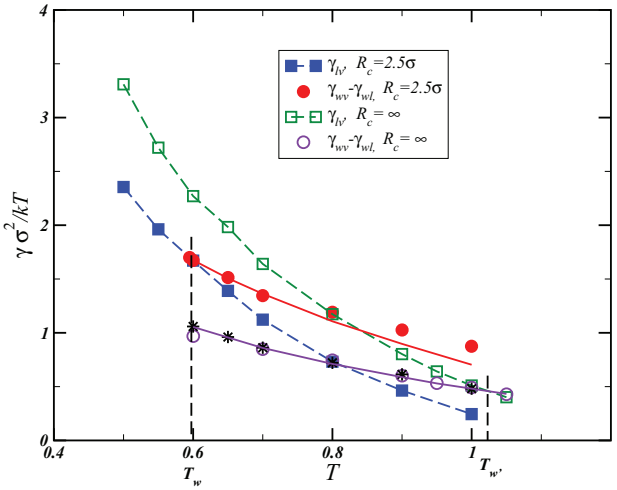

FIG. 4. Surface free energies versus temperature for Ar(g) adsorbed on $CO_2(s)$. Squares are liquid–vapor surface tensions, while circles are wall–vapor less wall–liquid free energies. Full symbols are results for truncated Ar–Ar interactions, while empty symbols denote results for the full model as obtained with SBC. Stars are results for $\gamma_{wv} - \gamma_{wl}$ as obtained with PSS–TC. Full lines are a fit to $\gamma_{wv} - \gamma_{wl} = k\Delta\rho$, with $k = 1.17\sigma\epsilon$ for ArCO2-TLJ, and $k = 0.718\sigma\epsilon$ for ArCO2-LJ. Dashed lines are a guide to the eye. Error bars are smaller than the size of the symbols.

SBC are expected to be of greater significance. Figure 3 shows density profiles for the model of Ar(g) adsorbed on $CO_2(s)$ that was described in Sec. III C, at a temperature of k_BT/ϵ=1.00. These profiles are obtained using a grand canonical simulation at coexistence chemical potential, and either liquid or vapor bulk densities imposed via the SBC. Two points are apparent here. First, the density profiles show no sign of discontinuity at the center of the simulation box. Second, the SBC are indeed capable of imposing exactly the expected bulk densities at the center of the pore. This is indicated in the figure by a black dashed line, which shows the coexistence densities obtained from bulk simulations.[51]

As a further test, we employed the wandering interface method (cf., Sec. III A) in order to calculate surface free energies for the solid–liquid and solid–vapor interfaces. Our results for the spreading coefficient, $\gamma_{wv} - \gamma_{wl}$, are presented in Fig. 4 for tail corrections evaluated using PSS (stars) and SBC (empty circles). The figure clearly shows that both methods are consistent, providing almost identical results within a large temperature range between $k_BT/\epsilon = 0.6$ and $k_BT/\epsilon = 1.0$. Relative to PSS, calculations of the energy using SBC are about a factor of 1/2 less time consuming. On the negative side, they require somewhat greater coding, and need the target bulk densities as input.

Having demonstrated the performance of SBC for the LJ fluid, we further note that the procedure can be applied immediately to polyatomic fluids provided one interprets the densities appearing in Eq. (18) as monomer densities. This is shown in Table I, which displays results for a Lennard–Jones dimer with bond distance $\ell = \sigma$ at a temperature $k_BT/\epsilon = 2.0$, explicit interactions truncated at $R_c = 2.5\sigma$ and tail corrections estimated with SSS, PSS, and SBC methods. As for the LJ case, the bulk internal energies obtained using SBC are very

close to the results obtained with SSS, while PSS slightly underestimates the internal energy by terms of order $1/D^3$.

B. Application to Ar adsorbed on CO_2

The model considered in this work is described in Sec. III C. In most computer simulation studies, it has been usual to study a related model, where the fluid–substrate interactions are as explained above, but the cohesive energy of Ar atoms is described with a Lennard–Jones potential spherically truncated at $R_c = 2.5\sigma$.[9–13,39,41] In what follows, we will denote this model as ArCO2-TLJ, in order to stress the fact that LJ interactions are truncated, while we will refer to the model originally considered by Ebner and Saam as ArCO2-LJ. To our knowledge, the only simulation study attempting to account for cohesive interactions beyond $R_c = 2.5\sigma$ is that of Sokołowsky and Fischer, who simulated the ArCO2-LJ model within the minimum image convention.[38]

1. Wetting temperature

A macroscopic adsorbed liquid film will wet a substrate whenever the surface free energy required to create a liquid–wall (γ_{wl}) and a liquid–vapor interface (γ_{lv}) is smaller than that required to form a single wall–vapor interface (γ_{wv}). Hence, one can locate the wetting transition by finding the temperature at which the following condition is first met

$$\gamma_{wv} - \gamma_{wl} \geq \gamma_{lv}. \tag{26}$$

In order to exploit this equation, we have calculated γ_{lv}, γ_{wv}, and γ_{wl}, using the WIM method with SBC as described in Sec. III A, for both the ArCO2-TLJ and the ArCO2-LJ models. In the latter case, the interactions beyond $R_c = 2.5\sigma$ are estimated using the SBC described in Sec. II C.

Figure 4 displays the results of surface free energies obtained from our simulations. The plot shows γ_{lv} (squares) and the difference $\Delta\gamma_w = \gamma_{wv} - \gamma_{wl}$ (circles) as a function of temperature for both the ArCO2-TLJ (full symbols) and the ArCO2-LJ (empty symbols) models.

For the ArCO2-TLJ model, the $\gamma_{lv}(T)$ curve shows a smooth monotonic decay towards the critical point as expected. For the case of $\Delta\gamma_w$, things are somewhat more difficult, due to capillary condensation effects. At temperatures below $k_BT/\epsilon = 0.6$, we could not obtain any further γ_{wl} surface free energies, because the system underwent capillary freezing. On the contrary, for temperatures above $k_BT/\epsilon = 0.7$, we could no longer calculate γ_{wv} because the system underwent capillary condensation. For that reason, the $\Delta\gamma_w$ curve is limited from below to temperatures $\sim 0.6\epsilon/k_B$, while the prolongation beyond $0.7\epsilon/k_B$ is possible by ignoring all together γ_{wv}, which at this temperature is still small. This explains the change of slope of $\Delta\gamma_w$ for the ArCO2-TLJ (red circles). Fortunately, these limitations do not prevent us from estimating the wetting temperature as the extrapolated crossing of γ_{lv} with $\Delta\gamma_w$ at a temperature slightly below $0.6\epsilon/k_B$, mainly, $\sim k_BT_w/\epsilon = 0.598$. This result is consistent with estimates by Errington, who suggested $k_BT_w/\epsilon = 0.598$ by extrapolation of the prewetting curve for data above $k_BT/\epsilon = 0.625$ (coincidentally, an agreement up to three digits is certainly more than could be expected from the accuracy of the measurements). Other estimates are less reliable because they extrapolate from above $k_BT/\epsilon = 0.7$ or more.[10,12]

For the ArCO2-LJ model, we encounter less problems and are able to calculate easily $\Delta\gamma_w$ for a large temperature range between $k_BT/\epsilon = 0.6$ and $k_BT/\epsilon = 1.05$. Beyond this temperature, the system undergoes a capillary condensation transition. However, this occurs only after γ_{lv} and $\Delta\gamma_w$ have crossed at a wetting temperature of about $k_BT_w/\epsilon = 1.02$. This result is indeed consistent with simulations by Sokołowsky and Fischer, who suggested a wetting temperature for the ArCO2-LJ model lying between $k_BT/\epsilon = 0.95$ and 1.00. Considering that these authors employed the minimum image convention in boxes with lateral dimensions of about $L = 10\sigma$, we can expect a slight underestimation of the cohesive LJ interactions that would slightly shift the wetting temperature below the exact result.

Obviously, one does expect that truncation of the LJ potential will affect the results obtained. Indeed, it is well known that the usual truncation at $R_c = 2.5\sigma$ shifts the critical point from about $k_BT_c/\epsilon = 1.33$ to $k_BT_c/\epsilon = 1.07$, i.e., somewhat less than 20%.[52,53] Also documented is the large contribution of neglected tail corrections in the liquid–vapor surface tension.[25,27,28,31,54] Such an effect is visible in Fig. 4, where clearly, γ_{lv} is about 30% larger for the ArCO2-LJ model with untruncated interactions. Our results show that a similar shift on $\Delta\gamma_w$ also occurs. However, in this case it is $\Delta\gamma_w$ for the ArCO2-TLJ which is much larger than that of the untruncated ArCO2-LJ model. These combined effects result in a huge shift of the wetting temperature of more than 40%.

2. Interface potentials

Considering the unexpected large shift of the wetting temperature, it seems safe to double-check the results with some alternative methodology. For this reason, we have calculated effective interface potentials (as described in Sec. III B) for both models at temperatures close to the wetting temperature predicted above.

Figure 5 shows results obtained for the ArCO2-TLJ model at temperatures $0.55\epsilon/k_B$ and $0.60\epsilon/k_B$. The results indicate that the system is far from wet at $0.55\epsilon/k_B$, since the free energy minimum corresponding to a thin adsorbed film is much lower than the free energy of an adsorbed liquid film. At $k_BT/\epsilon = 0.60$, however, we find the minimum has slightly raised above the free energy of the infinitely thick adsorbed film and the system is therefore slightly above the wetting temperature. These results are certainly consistent with a wetting temperature at $k_BT_w/\epsilon = 0.598$ as obtained from Young's equation.

As for the ArCO2-LJ model, Fig. 6 shows interface potentials for temperatures of $0.90\epsilon/k_B$ and $1.00\epsilon/k_B$. Similarly as before, the interface potentials show clearly that at $k_BT/\epsilon = 0.90$ the system is well below the wetting temperature, while, at $k_BT/\epsilon = 1.00$ the system seems to be slightly above the wetting temperature. In this case, it would seem that the method of interface potentials is predicting the wetting temperature

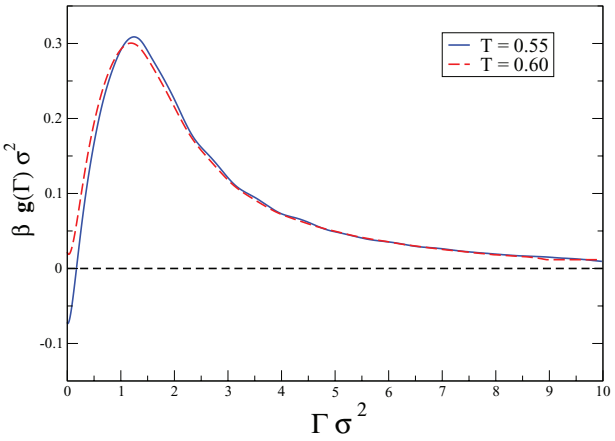

FIG. 5. Effective interface potentials obtained for the ArCO2-TLJ model at $k_BT/\epsilon = 0.55$ (full blue line) and $k_BT/\epsilon = 0.60$ (dashed red line).

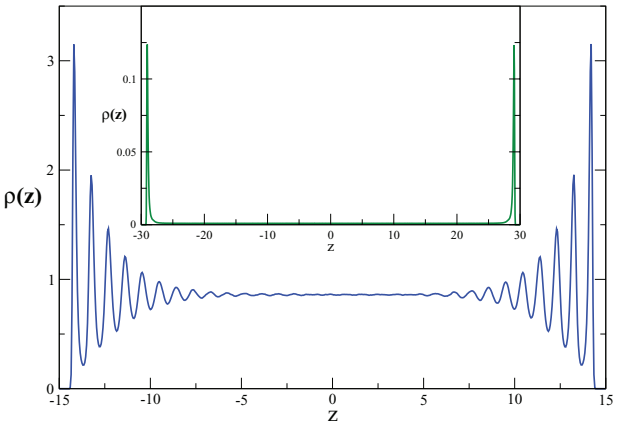

FIG. 7. Density profiles for the wall–liquid interface of the ArCO2-TLJ model at $k_BT/\epsilon = 0.60$ and coexistence conditions. The inset shows results for the wall–vapor interface.

somewhat below our results from Young's equation. However, taking into account the difficulty in sampling thick films of more than a thousand molecules, both sets of results may be considered to be in fair agreement.

Apart from being useful to determine the wetting temperature, a look at the interface potentials also reveals important differences between the ArCO2-LJ and ArCO2-TLJ models.

Figure 5 clearly shows that the adsorption of the thin film for the ArCO2-TLJ model is extremely small, both well below the wetting temperature and slightly above. Also in both cases it is apparent the very large activation barrier separating the thin to thick film regions. For the very modest lateral sizes considered in this work, the barrier amounts to $30k_BT$, which is indeed quite large. This easily explains why Monson and collaborators could not find thin to thick film transitions at temperatures well above the present estimate for the wetting temperature and hence, largely overestimated the wetting temperature.

In contrast with the ArCO2-TLJ model, Fig. 6 shows that the adsorption of the thin film for the ArCO2-LJ model is still small but indeed much larger, while the activation barrier for the wetting transition is significantly smaller.

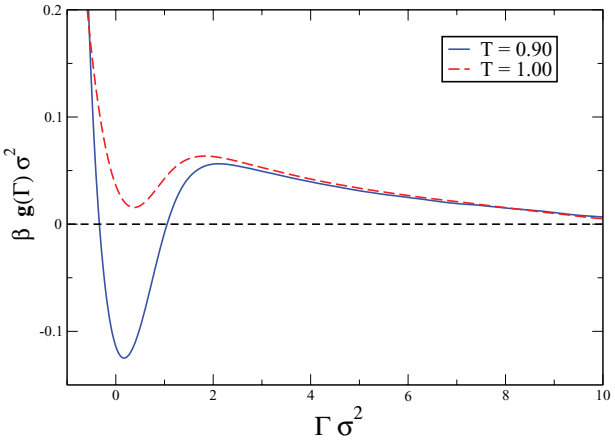

FIG. 6. Effective interface potentials obtained for the ArCO2-LJ model at $k_BT/\epsilon = =0.90$ (full blue line) and $k_BT/\epsilon = 1.00$ (dashed red line).

The difference in the structure of the wall–fluid interface at the wetting transition may be also discussed in terms of density profiles. Figure 7 shows the density profile of adsorbed vapor and liquid phases for the ArCO2-TLJ model at a temperature of $k_BT/\epsilon = 0.60$, very close to the wetting temperature. Compared with Fig. 3, which shows similar results for profiles close to the wetting temperature of ArCO2-LJ, we observe (i) the wall–liquid interphase is much more structured for the ArCO2-TLJ, with a first layer almost solid like (notice the very low density after the first maximum), and clear oscillatory correlations propagated for almost 10 molecular diameters. (ii) The wall–vapor interphase for the ArCO2-TLJ model shows an extremely small adsorption, with a single adsorbed peak one order of magnitude smaller than that of the liquid phase. On the other hand, for the ArCO2-LJ we observe (i) a less structured wall–liquid interphase with only a few strongly adsorbed layers and (ii) an incipient structured wall–vapor interphase, with two layers that have densities of equal order of magnitude than the liquid phase.

Overall, as could be expected, shifting the wetting transition to higher temperatures has the effect of considerably diminishing the strength of the transition, and also softens the structure of the interface.

V. DISCUSSION

In surface chemistry, the wetting transition is sometimes viewed as an interplay between cohesive and adhesive contributions, with wetting states resulting from stronger adhesive than cohesive forces. A decrease of the cutoff radius of the adsorbed fluid obviously decreases the cohesive energy of the bulk phases, hence, one expects the adhesive contributions will win over a larger range of temperatures, and hence, a decrease of the wetting temperature may be expected. These naive arguments may be possibly formulated more quantitatively using a simple sharp-kink approximation for the interfacial structure.[55] Under this approximation, the density profile

of a $\alpha\beta$ interface at z_0 is simply given by

$$\rho(z) = \begin{cases} \rho_\alpha & z < z_0 \\ \rho_\beta & z > z_0 \end{cases}, \tag{27}$$

where ρ_α and ρ_β stand for bulk coexistence densities of phases α and β, respectively. Then, using Eq. (15) for the interaction of a semi-infinite slab of phase β on a particle of phase α, one can readily calculate the energy per unit area that two semi-infinite slabs of α and β a distance ℓ apart feel[7]

$$U_{\alpha\beta}(\ell) = -\frac{\pi}{3}\rho_\alpha\rho_\beta\sigma_{\alpha\beta}^4\epsilon_{\alpha\beta}\left(\frac{\sigma_{\alpha\beta}}{\ell}\right)^2. \tag{28}$$

The surface free energies may then be estimated following Zisman as the work required to separate two chunks of α and β phases to infinity and joining them together a distance $\sigma_{\alpha\beta}$ apart in order to form two $\alpha\beta$ interfaces:[4,56,57]

$$\gamma_{\alpha\beta} = U_{\alpha\beta}(\sigma_{\alpha\beta}) - \frac{1}{2}(U_{\alpha\alpha}(\sigma_{\alpha\alpha}) + U_{\beta\beta}(\sigma_{\beta\beta})). \tag{29}$$

From these two equations, we can readily obtain estimates for γ_{lv}, γ_{wl}, and γ_{wv}, which, upon substitution into the condition for wetting, Eq. (26), yields an equation which is consistent with more formal arguments based on density functional theory (Ref. 4) and correctly describes the temperature dependence of contact angles[58]

$$\frac{\pi}{3}\sigma^4\epsilon(\rho_l - \rho_v)\left[\rho_w\frac{\sigma_w^4\epsilon_w}{\sigma^4\epsilon} - \rho_c\right] > \frac{\pi}{6}\sigma^4\epsilon(\rho_l - \rho_v)^2, \tag{30}$$

where ρ_c is the bulk critical density and we have further assumed $\rho_l + \rho_v = 2\rho_c$.

This is a quite remarkable result. It suggests that for a given fluid–substrate pair, purely bulk effects (namely, $\Delta\rho = \rho_l - \rho_v$) are sufficient to drive the wetting transition, since, eventually, $\Delta\rho$ must become small enough for the above condition to be satisfied as the bulk critical temperature is approached.

Of course, the irrelevant role of surface effects in this model stems from the assumption of structure less interfaces (cf., Eq. (27)). This assumption is quantitatively quite crude, but should be reasonable at a safe distance away from the critical point, where the bulk correlation length is still small compared to the molecular diameter. Including thermal effects into the model would certainly change the results, but one still expects that the purely bulk effect contained within $\Delta\rho = \rho_l - \rho_v$ is the leading contribution. Also note this equation incorporates explicitly the Cahn argument that a wetting transition will *always* occur before the critical temperature is reached,[59] since eventually $\Delta\rho^2$ must become sufficiently small compared to $\Delta\rho$, whence, the left-hand side of Eq. (30) must become larger than the right-hand side before the critical temperature is reached.

The arguments made above may be extended to the case where LJ interactions are truncated beyond a cutoff distance R_c, leading to the following condition for the wetting temperature:

$$\Delta\rho(T_w) = 2\rho_w\frac{\sigma_w^4\epsilon_w}{\sigma^4\epsilon}\chi(R_c/\sigma) - 2\rho_c, \tag{31}$$

where we have now included a factor $\chi(t)$ which accounts for the possibility of having the fluid–fluid interactions truncated beyond R_c, as in the ArCO2-TLJ model (see the Appendix):

$$\chi(t) = (1 - 4t^{-2} + 6t^{-3} - 3t^{-4})^{-1}. \tag{32}$$

For practical purposes, we can incorporate explicitly a temperature dependence into the above result by recalling the scaling assumption $\Delta\rho(T) = A(T_c - T)^\beta$, where T_c is the critical temperature and β now stands for a scaling exponent. The unknown prefactor may be determined by assuming the scaling law can be extrapolated down to the triple point (this apparently wild approximation is actually quite accurate for a LJ fluid). With this further assumption, we obtain the following closed expression for the wetting temperature:

$$\left(\frac{T_c - T_w}{T_c - T_t}\right)^\beta = \left(\frac{2\rho_w}{\Delta\rho_t}\frac{\sigma_w^4\epsilon_w}{\sigma^4\epsilon}\chi(R_c/\sigma) - \frac{2\rho_c}{\Delta\rho_t}\right), \tag{33}$$

where T_t and $\Delta\rho_t$ denote the temperature and liquid–vapor density difference at the triple point.

Equation (33) already explains qualitatively the large shift of wetting temperature when fluid–fluid interactions are truncated, since then $\chi(R_c/\sigma)$ is always larger than unity, and truncating the potential effectively amounts to a nominal increase of the adhesive contribution by a factor of $\chi(R_c/\sigma)$. For $R_c = 2.5\sigma$, we get that the adhesive contribution effectively increases by $\chi(2.5) = 1.5$.

Unfortunately, the model fails miserably when we use Eq. (33) in order to obtain absolute estimates of the wetting temperature. Indeed, considering that neither $\Delta\rho_t$ nor ρ_c change much with R_c, we can employ the known results $\rho_c\sigma^3 = 0.32$ (Ref. 51) and $\Delta\rho_t\sigma^3 = 0.84$ (Ref. 60) for the untruncated LJ. The ratio $(T_c - T_w)/(T_c - T_t)$ then takes the values of $2.6^{1/\beta}$ and $4.1^{1/\beta}$ for ArCO2–LJ and ArCO2–TLJ, respectively. This would imply that both models have wetting temperatures well below the triple point, which is certainly not the case at least for ArCO2–LJ.

The failure of the model is due mainly to a very poor estimate of γ_{lv}(right-hand side of Eq. (30)). On the other hand, the prediction that $\Delta\gamma_w = \gamma_{wv} - \gamma_{wl}$ is linear on $\Delta\rho$ (left-hand side of Eq. (30)) is actually very accurate. Depicted as continuous lines in Fig. 4 is a best fit of the form $\Delta\gamma_w = k\Delta\rho$, both for ArCO2-LJ and ArCO2-TLJ. The results are excellent for all the range of temperatures where reliable data are available, with $k = 0.718\sigma\epsilon$ and $k = 1.17\sigma\epsilon$, respectively.

Within the sharp-kink approach one finds for the constant

$$k(R_c/\sigma) = \frac{\pi}{3}\left(\rho_w\sigma_w^4\epsilon_w - \frac{\sigma^4\epsilon}{\chi(R_c/\sigma)}\rho_c\right). \tag{34}$$

For the ArCO2-LJ model, this yields $k(\infty) = 1.12\sigma\epsilon$, while for the ArCO2-TLJ model it gives $k(2.5) = 1.23\sigma\epsilon$. An estimate for the wetting temperature may then be given as the condition where $k\Delta\rho = \gamma_{lv}$. With the constant determined from the sharp-kink approximation and $\Delta\rho$, γ_{lv} obtained from simulation, we predict $T_w(\infty) = 0.88$ and $T_w(2.5) = 0.73$, and hence, a ratio $T_w(\infty)/T_w(2.5) = 1.2$, that compares with the simulation data of $T_w(\infty)/T_w(2.5) = 1.66$.

Obviously, this model is a rather crude caricature of the expected Ar–Ar and Ar–CO_2 interactions. Indeed, there is a small but significant role of three body forces in Ar,[61] while the Ar–CO_2 interactions are considerably anisotropic and strongly favor the perpendicular approach of Ar to CO_2.[62]

Furthermore, the CO_2 surface is possibly above the roughening transition, and some limited adsorption of Ar on bulk CO_2 may be expected. However, the goal of this paper is not to provide an accurate modeling of this system, but rather, to highlight the role of truncated van der Waals interactions.

Our theoretical considerations, together with the simulation results, clearly show the large influence of van der Waals tails in the location of the wetting transition. This does not necessarily mean, however, that such tails must be included in order to properly model a fluid–substrate pair. In most cases, both the fluid–fluid and fluid–substrate interactions are described with a crude empirical model, and the neglect of tail corrections may very well remedy for other deficiencies. Actually, the experimental study of Ar/CO_2 reveals triple point wetting,[63] a behavior which is actually closely followed by the ArCO2–TLJ, and certainly not for the ArCO2–LJ. This fact is consistent with claims that the Ar–CO_2 interactions in the Ebner–Saam model are much too weak,[63] and support our conclusion that truncating the fluid potential effectively amounts to increasing the fluid–substrate interaction (cf., Eq. (33)).

VI. CONCLUSIONS

In this work we suggest a method to account for long tail dispersive interactions which implicitly mimics SBC appropriate for the study of the interface between two macroscopic bulk phases. The results obtained are in agreement with those obtained using related methods, but the SBC suggested here are physically appealing and somewhat reduce the computational cost. The method proposed may be readily applied to the study of adsorbed fluid phases, but is still unclear how to exploit for the study of free interfaces. It must also be stressed that the assumption of a density profile $\rho(\mathbf{r}) = \rho(z)$ that is only inhomogeneous in one direction is exact on the average, but not *instantaneously*. The method therefore incorporates a mean-field character to the simulations. Particularly, it cannot deal with the presence of lateral capillary waves, which have the effect of considerably blurring the density profiles.[64] Fortunately, for systems with typical lateral sizes employed in simulation, such effect should be quite small provided one studies systems away from the critical point.

We have calculated surface free energies for liquid–vapor, wall–liquid, and wall–vapor interfaces for selected systems using the WIM.[42] Such free energies may be obtained over a large temperature interval and exploited in order to reliably obtain wetting temperatures using Young's equation (cf., Refs. 14, 18, and 47). This method is far more robust than that of searching for the intersection of prewetting and vapor pressure lines.[13,14,47,65] The reason is that the spreading coefficient, $\gamma_{wv} - \gamma_{wl}$ easily intersects with γ_{lv} and may, in principle, even be calculated beyond a first order wetting transition (in practice, simulations meet the problem of capillary condensation/evaporation). On the contrary, it is impossible to calculate prewetting lines close to the wetting temperature, because the coexisting thick film diverges. As a result, intersection of the prewetting and vapor pressure lines requires unreliable extrapolation, as is apparent from estimates by Shi *et al.*, who have argued that wetting temperatures differing as much as 30% may be obtained depending on the extrapolation scheme employed.[12]

Using the methods described above, we calculated wetting temperatures for a model of Argon adsorbed on solid CO_2, both under semi-infinite boundary conditions (i.e., full long tail corrections for the Ar–Ar interactions) and for a system with truncated Ar–Ar interaction at the "conventional" value of $R_c = 2.5\sigma$. Our results show a dramatic effect of the neglected long tail corrections, with the wetting temperature shifting from $k_B T_w/\epsilon = 1.0$ to $k_B T_w/\epsilon = 0.6$. Intriguingly, the behavior of the model with truncated interactions follows the experimentally observed wetting behavior much closer than that with full dispersive interactions.[63]

ACKNOWLEDGEMENTS

We would like to thank Marcus Müller for suggesting us to describe the cutoff dependence of wetting properties by means of the sharp-kink approximation (cf., Sec. V). We also benefitted from helpful discussions with P. Bryk, A. Archer, and E. de Miguel. Generous financial support of Ministerio de Educacion y Ciencia through Project Nos. FIS2010-22047-C05-05 and FIS2010-14866; Comunidad Autonoma de Madrid through Project No. MODELICO-P2009/ESP-1691; and Junta de Andalucia through Project No. P07-FQM02884 is gratefully acknowledged.

APPENDIX: SHARP KINK APPROXIMATION FOR TRUNCATED INTERACTIONS

The energy felt by a molecule α with truncated LJ potential due to β molecules uniformly distributed on a plane a distance z away is

$$w_{\alpha\beta}(z; R_c) = \int_{\mathbf{r}_\parallel \in \mathfrak{C}(r_\parallel^{max}, z_i)} u_{\alpha\beta}(\mathbf{r}_i, \mathbf{r})\, \mathrm{d}\mathbf{r}_\parallel, \tag{A1}$$

where $r_\parallel^{max} = (R_c^2 - z^2)^{1/2}$ for $z < R_c$ and zero otherwise. The result of this integration is

$$w_{\alpha\beta}(z; R_c) = w_{\alpha\beta}(z; \infty) - w_{\alpha\beta}(R_c; \infty), \tag{A2}$$

where $w_{\alpha\beta}(z; \infty)$ denotes the slice potential of Eq. (5). From this equation we readily obtain the energy per unit area between two semi-infinite slabs of α and β a distance ℓ apart

$$U_{\alpha\beta}(\ell; R_c) = \rho_\alpha \rho_\beta \int_{-\infty}^{0} \mathrm{d}z' \int_{\ell}^{\infty} \mathrm{d}z\, w_{\alpha\beta}(z' - z; R_c). \tag{A3}$$

Integration yields

$$U_{\alpha\beta}(\ell; R_c) = U_{\alpha\beta}(\ell; \infty) - U_{\alpha\beta}(R_c; \infty) - \frac{1}{4}\rho_\alpha \rho_\beta \sigma_{\alpha\beta}^2 w_{\alpha\beta}(R_c; \infty) \left(\frac{\ell}{\sigma_{\alpha\beta}} - \frac{R_c}{\sigma_{\alpha\beta}} \right)^2, \tag{A4}$$

where $U_{\alpha\beta}(\ell; \infty)$ denotes here Eq. (28). Using the above result we can then obtain surface free energies from Eq. (29),

yielding

$$\gamma_{\alpha\beta} = \rho_\alpha \rho_\beta \sigma_{\alpha\beta}^4 \epsilon_{\alpha\beta} f(R_c/\sigma_{\alpha\beta}) - \frac{1}{2} \times \left[\rho_\alpha^2 \sigma_{\alpha\alpha}^4 \epsilon_{\alpha\alpha} f(R_c/\sigma_{\alpha\beta}) + \rho_\beta^2 \sigma_{\beta\beta}^4 \epsilon_{\beta\beta} f(R_c/\sigma_{\beta\beta})\right], \quad \text{(A5)}$$

where

$$f(t) = -\frac{\pi}{3}[1 - 4t^{-2} + 6t^{-3} - 3t^{-4}] \quad \text{(A6)}$$

By use of Eq. (A5) into Young's equation we obtain the result of Eq. (31).

[1] M. Allen and D. Tildesley, *Computer Simulation of Liquids* (Clarendon, Oxford, 1987).
[2] D. Frenkel and B. Smit, *Understanding Molecular Simulation*, 2nd ed. (Academic, San Diego, 2002).
[3] A. A. Chernov and L. V. Mikheev, Phys. Rev. Lett. **60**, 2488 (1988).
[4] M. Schick, *Liquids at Interfaces*, Les Houches Lecture Notes (Elsevier, Amsterdam, 1990), pp. 1–89.
[5] J. R. Henderson, Phys. Rev. E **50**, 4836 (1994).
[6] J. R. Henderson, Phys. Rev. E **72**, 051602 (2005).
[7] J. N. Israelachvili, *Intermolecular and Surfaces Forces*, 2nd ed. (Academic, London, 1991).
[8] J. H. Sikkenk, J. O. Indekeu, J. M. J. van Leeuwen, and E. O. Vossnack, Phys. Rev. Lett. **59**, 98 (1987).
[9] J. E. Finn and P. A. Monson, Mol. Phys. **65**, 1345 (1988).
[10] J. E. Finn and P. A. Monson, Phys. Rev. A **39**, 6402 (1989).
[11] M. B. Sweatman, Phys. Rev. E **65**, 011102 (2001).
[12] W. Shi, X. Zhao, and J. K. Johnson, Mol. Phys. **100**, 2139 (2002).
[13] J. R. Errington, Langmuir **20**, 3798 (2004).
[14] L. G. MacDowell and M. Müller, J. Chem. Phys. **124**, 084907 (2006).
[15] S. Toxvaerd, J. Phys. Chem. C **111**, 15621 (2007).
[16] S. Peter, H. Meyer, and J. Baschnagel, J. Chem. Phys. **131**, 014902 (2009).
[17] S. Peter, H. Meyer, and J. Baschnagel, J. Chem. Phys. **131**, 014903 (2009).
[18] V. Kumar, S. Sridhar, and J. R. Errington, J. Chem. Phys. **135**, 184702 (2011).
[19] K. F. Mansfield and D. N. Theodorou, Macromolecules **23**, 4430 (1990).
[20] K. F. Mansfield and D. N. Theodorou, Macromolecules **24**, 4295 (1991).
[21] M. Mecke, J. Winkelmann, and J. Fischer, J. Chem. Phys. **107**, 9264 (1997).
[22] M. Mecke, J. Winkelmann, and J. Fischer, J. Chem. Phys. **110**, 1188 (1999).
[23] F. Siperstein, A. L. Myers, and O. Talu, Mol. Phys. **100**, 2025 (2002).
[24] K. C. Daoulas, V. A. Harmandaris, and V. G. Mavrantzas, Macromolecules **38**, 5780 (2005).
[25] J. Janecek, J. Phys. Chem. B **110**, 6264 (2006).
[26] J. Janecek, H. Krienke, and G. Schmeer, J. Phys. Chem. B **110**, 6916 (2006).
[27] V. K. Shen, R. D. Mountain, and J. R. Errington, J. Phys. Chem. B **111**, 6198 (2007).
[28] L. G. MacDowell and F. J. Blas, J. Chem. Phys. **131**, 074705 (2009).
[29] M. Guo and B. C.-Y. Lu, J. Chem. Phys. **106**, 3688 (1997).
[30] F. Goujon, P. Malfreyt, A. Boutin, and A. H. Fuchs, J. Chem. Phys. **116**, 8106 (2002).
[31] C. Ibergay, A. Ghoufi, F. Goujon, P. Ungerer, A. Boutin, B. Rousseau, and P. Malfreyt, Phys. Rev. E **75**, 051602 (2007).
[32] A. Ghoufi, F. Goujon, V. Lachet, and P. Malfreyt, J. Chem. Phys. **128**, 154716 (2008).
[33] C. Ebner and W. F. Saam, Phys. Rev. Lett. **38**, 1486 (1977).
[34] R. Evans and P. Tarazona, Phys. Rev. A **28**, 1864 (1983).
[35] T. F. Meister and D. M. Kroll, Phys. Rev. A **31**, 4055 (1985).
[36] E. Velasco and P. Tarazona, Phys. Rev. A **42**, 2454 (1990).
[37] M. Zeng, J. Mi, and C. Zhong, Phys. Rev. B **82**, 125452 (2010).
[38] S. Sokolowski and J. Fischer, Phys. Rev. A **41**, 6866 (1990).
[39] Y. Fan and P. W. Monson, J. Chem. Phys. **99**, 6897 (1993).
[40] M. J. Bojan, G. Stan, S. Curtarolo, W. A. Steele, and M. W. Cole, Phys. Rev. E **59**, 864 (1999).
[41] J. R. Errington and D. W. Wilbert, Phys. Rev. Lett. **95**, 226107 (2005).
[42] L. G. MacDowell and P. Bryk, Phys. Rev. E **75**, 061609 (2007).
[43] R. Evans and U. M. B. Marconi, J. Chem. Phys. **87**, 7138 (1987).
[44] J. R. Henderson, in *Fundamentals of Inhomogenous Fluids*, edited by D. Henderson (Marcel Dekker, New York, 1992), Chap. 2, pp. 23–84.
[45] B. Smit, Mol. Phys. **85**, 153 (1995).
[46] K. Binder, Phys. Rev. A **25**, 1699 (1982).
[47] M. Müller and L. G. MacDowell, Macromolecules **33**, 3902 (2000).
[48] L. G. MacDowell, Euro. Phys. J. Spec. Top. **197**, 131 (2011).
[49] M. Fitzgerald, R. R. Picard, and R. N. Silver, Europhys. Lett. **46**, 282 (1999).
[50] P. Attard, Mol. Phys. **104**, 1951 (2006).
[51] A. Lotfi, J. Vrabec, and J. Fischer, Mol. Phys. **76**, 1319 (1992).
[52] B. Smit, J. Chem. Phys. **96**, 8639 (1992).
[53] A. Trokhymchuk and J. Alejandre, J. Chem. Phys. **111**, 8510 (1999).
[54] G. Galliero, J. Chem. Phys. **133**, 074705 (2010).
[55] M. Mueller, private communication (2009).
[56] W. A. Zisman, Adv. Chem. Ser. **43**, 1 (1964).
[57] P. G. de Gennes, Rev. Mod. Phys. **57**, 827 (1985).
[58] R. García, K. Osborne, and E. Subashi, J. Phys. Chem. B **112**, 8114 (2008).
[59] J. W. Cahn, J. Chem. Phys. **66**, 367 (1977).
[60] E. A. Mastny and J. J. de Pablo, J. Chem. Phys. **127**, 104504 (2007).
[61] J. A. Anta, E. Lomba, and M. Lombardero, Phys. Rev. E **55**, 2707 (1997).
[62] P. J. Marshall, M. M. Szczesniak, J. Sadlej, G. Chalasinski, M. A. ter Horst, and C. J. Jameson, J. Chem. Phys. **104**, 6569 (1996).
[63] G. Mistura, F. Ancilotto, L. Bruschi, and F. Toigo, Phys. Rev. Lett. **82**, 795 (1999).
[64] E. M. Fernández, E. Chacón, and P. Tarazona, Phys. Rev. E **84**, 205435 (2011).
[65] M. Müller and L. G. MacDowell, J. Phys.: Condens. Matter **15**, R609 (2003).